Role of SRP19 in Assembly of the *Archaeoglobus fulgidus* Signal Recognition Particle†

John L. Diener and Charles Wilson*

Department of Biology and Center for the Molecular Biology of RNA, Sinsheimer Laboratories, University of California at Santa Cruz, Santa Cruz, California 95064

Received May 24, 2000; Revised Manuscript Received August 23, 2000

ABSTRACT: Previous studies have shown that SRP19 promotes association of the highly conserved signal peptide-binding protein, SRP54, with the signal recognition particle (SRP) RNA in both archaeal and eukaryotic model systems. In vitro characterization of this process is now reported using recombinantly expressed components of SRP from the hyperthermophilic, sulfate-reducing archaeon *Archaeoglobus fulgidis*. A combination of native gel mobility shift, filter binding, and Ni-NTA agarose bead binding assays were used to determine the binding constants for binary and ternary complexes of SRP proteins and SRP RNA. Archaeal SRP54, unlike eukaryotic homologues, has significant intrinsic affinity for 7S RNA ($K_D \sim 15$ nM), making it possible to directly compare particles formed in the presence and absence of SRP19 and thereby assess the precise role of SRP19 in the assembly process. Chemical modification studies using hydroxyl radicals and DEPC identify nonoverlapping primary binding sites for SRP19 and SRP54 corresponding to the tips of helix 6 and helix 8 (SRP19) and the distal loop and asymmetric bulge of helix 8 (SRP54). SRP19 additionally induces conformational changes concentrated in the proximal asymmetric bulge of helix 8. Selected nucleotides in this bulge become modified as a result of SRP19 binding but are subsequently protected from modification by formation of the complete complex with SRP54. Together these results suggest a model for assembly in which bridging the ends of helix 6 and helix 8 by SRP19 induces a long-range structural change to present the proximal bulge in a conformation compatible with high-affinity SRP54 binding.

The proper function of a diverse assortment of proteins, including channels, pumps, receptors, toxins, and hormones, requires their insertion into or transport across cellular membranes. Translation and targeting of membrane bound or secreted proteins are coupled by the action of a ribonucleoprotein complex (RNP)[1] called the signal recognition particle (SRP) (for a review, see ref *1*). The mammalian SRP complex is composed of six polypeptides (*2*) and an ∼300 nucleotide, RNA (*3*). Many of the functions of the SRP complex can be ascribed to a single protein, SRP54, whose homologue appears to be the only protein component of most bacterial particles. The consensus secondary structure of the SRP RNA from *Eukarya* and *Archaea* (*4*) contains four helical domains, numbered I−IV (Figure 1) (*5*−*8*). In contrast, most bacterial SRP RNA sequences contain only a single domain (domain IV), which contains the most conserved regions of the signal binding domain of SRP RNA (*7*, *9*, *10*). While subcellular structure differs enormously between the three domains of life, biochemical evidence suggests that SRP provides the same basic role in translocation in *Archaea* as in *Bacteria* and *Eukarya* (*11*).

In vitro reconstitution experiments using mammalian SRP components have shown that the highly conserved SRP54 protein requires a second factor, SRP19, to assemble with SRP RNA (*12*). In contrast, the bacterial SRP54 homologue (*ffh*, fifty-four homologue) can bind either bacterial or human SRP RNA in the absence of any accessory proteins (*13*, *14*). Low-resolution mapping of mammalian SRP RNA using the nuclease α-sarcin identified the tips of domains III and IV (helix 6 and helix 8) as sites that are protected by addition of SRP19 (*15*). Sequence homology searches of complete bacterial and archaeal genomes thus far suggest that SRP19 homologues are found only in organisms whose SRP RNAs also contain helix 6 (*9*), consistent with the proposal that SRP19-mediated SRP54 assembly involves cooperative interactions between helix 6 and helix 8. It has been shown recently that an SRP19 homologue identified in the genome of *Archeoglobus fulgidus* is capable of binding SRP RNA and promoting incorporation of the SRP54 protein into the complex (*16*). In contrast to the mammalian complex, an SRP54−SRP RNA partial complex can form (with reduced efficiency) in the absence of SRP19. A detailed understanding of the mechanism for SRP assembly and the reasons for the apparent differences between particles across the domains of life has remained lacking for the several reasons outlined below.

Structural analysis of SRP has mainly been concentrated on components of the bacterial particle, with the notable exceptions of the crystal structure of the human SRP54 methionine rich or "M-domain" (*17*) and the N-terminal and

† This work is supported by a grant to C.W. from the Packard Foundation. J.D. is supported by an NSF/Alfred P. Sloan Foundation Postdoctoral Research Fellowship in Molecular Evolution.

* To whom correspondence should be addressed. E-mail: wilson@biology.ucsc.edu. Phone: (831) 459-5126. Fax: (831) 459-3139.

[1] Abbreviations: SRP, signal recognition particle; DEPC, diethylpyrocarbonate; Ni-NTA, nickel-nitrilotriacetic acid; EDTA, ethylenediaminetetraacetic acid; SDS, sodium dodecyl sulfate; PAGE, polyacrylamide gel electrophoresis.

10.1021/bi001180s CCC: $19.00
Published on Web 09/30/2000

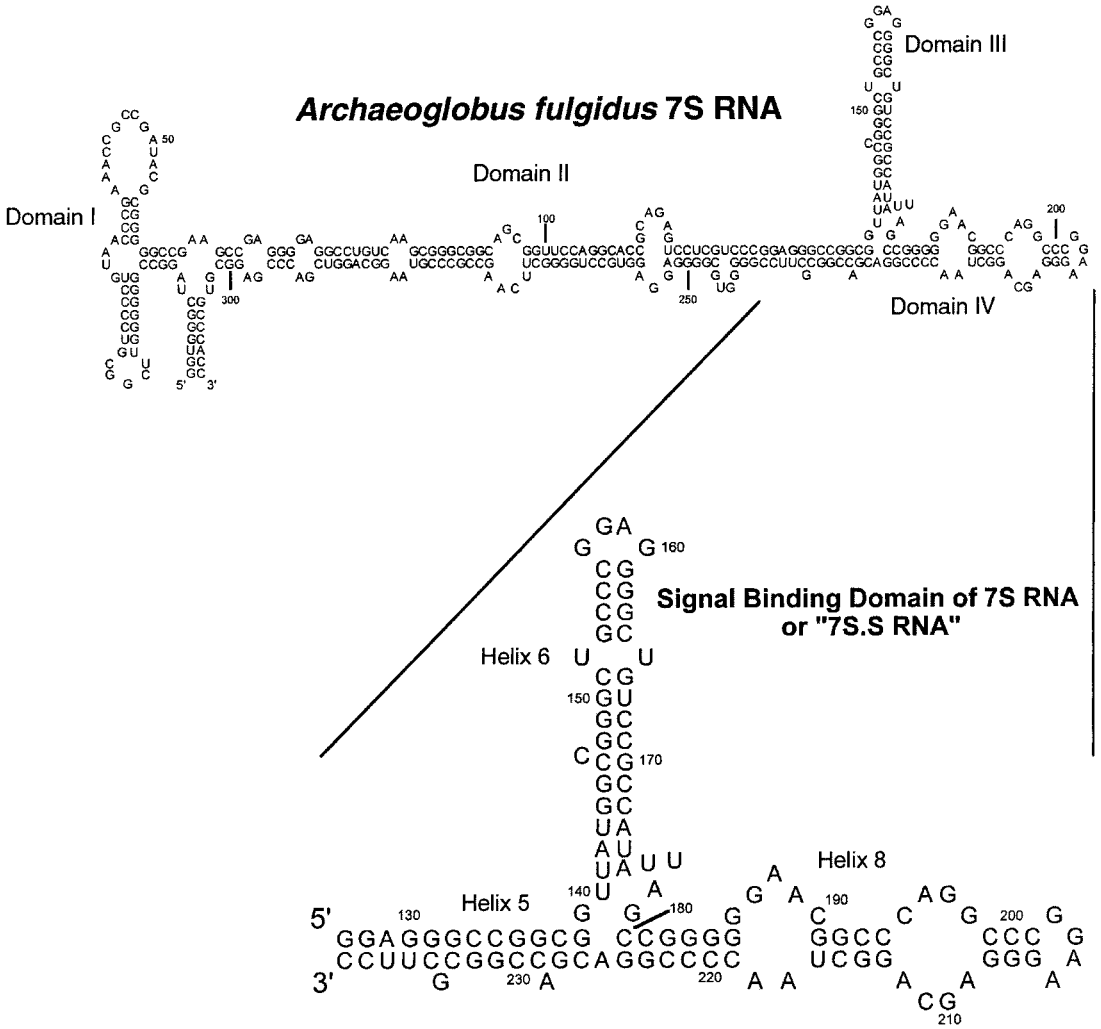

FIGURE 1: Secondary structures of *Archaeoglobus Fulgidus* 7S RNA and the signal binding domain RNA construct, 7S.S RNA.

GTPase domain of an archaeal SRP54 (*18*). While crystal and/or solution structures are now available for helix 8 (*19*−*21*), for the *ffh* protein (*22*, *23*), and for a complex formed by fragments of each (*24*), these do not directly inform on the assembly process to the extent that bacterial SRP does not require a specific assembly factor. The inability of mammalian SRP54 to detectably interact with its RNA target further complicates analysis of assembly in that it is impossible to directly observe how SRP19 alters the nature of their interaction. While a number of qualitative binding studies have been carried out with the mammalian SRP (*14*, *25*−*32*) and more recently with the archaeal SRP (*16*), no quantitative information on the affinities of the various protein-RNA complexes is currently available, as it is for bacterial particles (*33*−*35*). Eukaryotic SRP19- and SRP54-binding sites have been mapped using a series of engineered mutations of the SRP RNA (*27*, *28*, *36*). In this type of analysis, however, it is formally impossible to distinguish modifications that directly block protein binding from those that promote misfolding of the RNA and thus inhibit protein binding indirectly. As noted previously, enzymatic probing has been used to characterize protein binding to the eukaryotic SRP at low resolution. The α-sarcin footprint of canine SRP19−SRP54−SRP RNA is indistinguishable from that of SRP19−SRP RNA (*15*), leading to the early suggestion that SRP54 was indirectly bound to the particle via SRP19. However, subsequent observations have been made in which hybrid *E. coli*-mammalian SRPs could spontaneously assemble. That the bacterial SRP54 homologue binds the mammalian SRP RNA (*14*) and that the mammalian SRP54 specifically binds *E. coli* SRP RNA (*13*, *37*) argue instead that this protein likely interacts directly with SRP RNA, leaving an open question: why is SRP19 required for assembly of the eukaryotic particle?

To understand both the mechanism of RNP assembly and the evolution of the assembly process, we have characterized SRP from the sulfate-reducing archaeon *Archaeoglobus fulgidus* (*38*). Like many archaeal species, *A. fulgidus* is an extremophile and has an optimal growth temperature of 83 °C (*38*). The ability of many of the *Archaea* to survive in extremes of temperature, salt, and pH often results in an increased stability of their biomolecules and corresponding complexes, making them excellent model systems for structural analysis. The ability of the archaeal particle to assemble with reduced efficiency in the absence of SRP19 makes it uniquely possible to characterize the specific conformational differences between the partially and fully assembled SRP states using chemical probing. Direct analysis of the binding sites of SRP19, SRP54, and the C-terminal SRP54 methionine rich or M-domain yields a schematic

model for archaeal SRP assembly and a hypothesis for the different assembly requirements observed for the particle in the three domains of life.

MATERIALS AND METHODS

Preparation of RNA and Proteins. Plasmids containing the genes for 7S RNA, SRP19 and SRP54 homologues from *A. fulgidus* were purchased from the American Type Culture Collection.

PCR was performed on respective plasmids using oligodeoxynucleotide primers 5′-GATCGGGAATTCCATATGAAGGAGTGCGTTGTCTGG (upstream SRP19), 5′-GATCCGCTCTTCCGCATTTCTTCTTCTTCTTTTTCTTGT (downstream SRP19), 5′-GATCGGGAATTCCATATGGCTCTTGAATCTCTCAA (upstream SRP54), 5′-GATCGGATCCTCATCATCA*ATGATGATGATGATGATG*GAAACCCAGCTTCCCCAGAC (downstream SRP54), 5′GATCGGGAATTCCATATGGGCGAAGCATTCCT GAAGGGA-3′ (upstream SRP54-M domain which begins at SRP54 residue 309 and generates a polypeptide homologous to that solved by crystallography (*17*)), 5′GATCGGGAATTCCATATGGAATAATACGACTCACTATAGGTGGGCTAGGCCGGGGGGT (upstream 7S RNA), 5′-GATCGAATTCGATCCTCTTCA GGTGGGCACGCCTCGGGTCG (downstream 7S RNA), 5′-GATCGGG AATTCCATATGGAA**TAATACGACTCACTATA**GGAGGGCCGGCGG TTATGGC (upstream 7S.S RNA), 5′-GATCGAATTCGATCCTCTTCAGGAAGCGCC GGTCGTCCGGG (downstream 7S.S) (restriction sites, the His-6 tag and T7 promoters used are underlined, italicized and bolded, respectively). All PCR was performed with Vent DNA polymerase (New England Biolabs) at 1 unit/μL in reactions containing 0.2 mM dNTPs, 10 mM KCl, 10 mM ammonium sulfate, 20 mM Tris-HCl (pH 8.8 at 298 °C), 3 mM MgSO4, 0.1% Triton-X 100, 1−3 μM primers, and ∼1 ng of plasmid template (SRP54-M domain used the SRP54 downstream primer and RNA genes also required 5% DMSO).

All restriction enzymes and T4 DNA ligase were purchased from New England Biolabs. The SRP19 PCR product was double digested with *Nde*I and *Sap*I restriction enzymes and ligated into *Nde*I/*Sap*I-digested pTYB1 plasmid insert (IMPACT T7 System from New England Biolabs), which contains an intein/chitin binding protein fusion in frame and C-terminal to the SRP19 insert. The SRP54 and SRP54M PCR products were double digested with *Nde*I and *Bam*HI restriction enzymes and ligated into *Nde*I/*Bam*HI digested pET-21-b plasmid (Novagen). The PCR products for both 7S and 7S.S RNAs were digested with *Nde*I and *Eco*RI and ligated into *Nde*I/*Eco*RI digested pT7blue plasmid (Novagen). The RNA genes were later sub-cloned into the pUC-118 plasmid (United States Biochemical) using *Hin*dIII and *Eco*RI restriction sites common to both plasmids. Plasmid products were all transformed into the *E. coli* DH5-α strain and selected via ampicillin resistance (200 μg/mL). Clones were either sequenced manually using the T7 Sequenase V 2.0 kit (Amersham) or by Genemed Synthesis, South San Francisco California.

RNA was transcribed by T7 RNA polymerase (*39*) from purified plasmid, which had been previously digested with the restriction enzyme *Ear*I at a concentration of 65 μg of plasmid/mL of transcription reaction. Products were purified on 10% denaturing polyacrylamide gels and eluted overnight via the crush and soak method. Final RNA concentrations were calculated using the measured absorbance at 260 nm.

SRP19 and SRP54 and SRP54-M domain DNA contain a large number of rare arginine codons. We thus used BL21 Codon Plus (DE3)-RIL competent cells (Stratagene) to improve expression yields. Cultures were grown at 37 °C to 0.5 OD in the presence of both 100 μg/mL ampicillin and induced with 1 mM IPTG. SRP19 cultures were induced overnight at 20 °C while SRP54 and SRP54-M domain cultures were induced for 5 h at 37 °C. SRP19 was purified to >95% purity using the Impact-T7 kit (New England Biolabs). Clarified SRP19 lysate was applied to chitin resin (New England Biolabs) at 4 °C and washed with 500 mM NaCl, 20 mM Na-Hepes, pH 7.5, 0.1% Triton X-100, and 1 mM EDTA. The protein-bound resin was then incubated ∼36 h at 37 °C with 100 mM DTT, 200 mM NaCl, 20 mM Na-Hepes, pH 7.5, 0.1% Triton X-100, and 1 mM EDTA. The cleaved SRP19 protein was eluted from the column with 5 mM DTT, 1 M NaCl, 20 mM Na-Hepes, pH 7.5, and 1 mM EDTA. Purified protein was dialyzed into 20 mM K-Hepes, pH 7.5, 100 mM KCl, 5 mM $MgCl_2$, 1 mM DTT, and 10% glycerol, analyzed by SDS−PAGE and stored at −20 °C. SRP54 and SRP54-M were purified to >90% purity under native conditions with Ni-NTA agarose resin using the standard Qiagen protocol. Purified protein was dialyzed into a final buffer containing 20 mM K-Hepes, pH 7.5, 100 mM KCl, 5 mM $MgCl_2$, 1 mM DTT, and 10% glycerol. Final protein concentrations were determined using the Bradford Assay (Bio-Rad).

Protease Cleavage Reactions. Binding reactions were carried out using a method reported previously for mobility shift assays of thermophilic L1 ribosomal protein−RNA complexes (*40*). 20 μL reactions contained 20 mM K-Hepes, pH 7.5, 100 mM KCl, 5 mM $MgCl_2$, 1 mM DTT, 0.1 mM EDTA, and 10% glycerol in addition to trace 5′-^{32}P-end-labeled-7S RNA (<20 pM for all reactions), 1 mg/mL tRNA and 1 mg/mL BSA as competitors and/or SRP19 and SRP54 at various concentrations. Reactions were performed in duplicate. Following incubation at 65 °C for 15 min, 1 μL of 20 mM $CaCl_2$ with or without 20 mg/mL proteinase-K (Promega) was added to each reaction. Reactions were then incubated for 15 min at 37 °C followed by fractionation on a 6% (49:1 acrylamide:bis-acrylamide) native polyacrylamide gel at 5 W at 4 °C for 1.5 h.

Protease Protection Reactions. Twenty microliter binding reactions were prepared in 20 mM K-Hepes, pH 7.5, 100 mM KCl, 5 mM $MgCl_2$, 1 mM DTT, 0.1 mM EDTA, 1 mg/mL tRNA, 50 μg/mL BSA, and ∼1 μM SRP19 (∼10 μg/mL), with or without 1 μM 7S.S RNA. Reactions were incubated for 15 min at 65 °C followed by addition of 1 μL of 20 mg/mL proteinase-K in 20 mM $CaCl_2$, incubation for 15 min at 37 °C, and fractionation by SDS−PAGE with Coomassie staining.

Isolation of the Archaeal SRP Complex via Ni-NTA Agarose Bead Binding. One hundred microliter binding reactions were prepared using buffers and conditions detailed above and contained 1 mg/mL tRNA. Reactions also contained 1 μM concentrations of either SRP19 + BSA, SRP19 + 7S.S RNA + BSA, SRP19 + SRP54 + BSA or SRP19 + 7S.S RNA + SRP54 + BSA. Following 15 min of incubation at 65 °C, 20 μL of a 50% slurry of Ni-NTA

agarose beads (Qiagen) which had been pre-equilibrated in binding buffer (20 mM K-Hepes, pH 7.5, 100 mM KCl, 5 mM $MgCl_2$, 1 mM DTT, 0.1 mM EDTA, and 10% glycerol) was added. The binding capacity of 10 μL of Ni-NTA beads is ~3−5 nmol, thus the Ni-NTA-binding sites were in ~30−50-fold molar excess over SRP54. Reactions were incubated with beads on ice for 30 min followed by spin filtering with Spin-X 0.2 μm micro filters (Costar) and three washes with 400 μL of the binding buffer described above, 400 μL of the binding buffer + 10 mM imidazole, and 400 μL of the binding buffer + 20 mM imidazole to remove any nonspecific protein binding to the beads. Samples were eluted with 50 μL of 500 mM imidazole, pH 7, lyophilized, resuspended in SDS loading buffer, analyzed by 15% SDS−PAGE, and stained with Coomassie.

Native Gel Electrophoresis. Trace 5′-^{32}P-end-labeled-7S RNA concentrations were estimated assuming 100% theoretical yield of input unlabeled RNA through labeling, gel purification, and elution. Reactions were prepared as described above and equilibrated at 65 °C for 15 min and fractionated on a 6% (49:1 acrylamide:bis-acrylamide) native polyacrylamide gel at 5 W at 4 °C for 1.5 h. Bands were analyzed using a Molecular Dynamics phosphorimager. The fraction bound was estimated by quantifying the free and bound bands indicated in Figure 3 and computing the ratio of bound/(free + bound).

Filter Binding Assays. Binding reactions for filter binding assays carried out as described above for protease cleavage reactions and native gel mobility shift assays. After incubation at 65 °C for 15 min, reactions were chilled on ice. Nitrocellulose filters (0.45 μm from Millipore) were pre-equilibrated with binding buffer. The 20 μL binding reactions were drawn through the filters under vacuum and followed immediately by a wash with 5 mL (250 reaction volumes) ice-cold binding buffer. Filters were air-dried, resuspended in 3 mL of Complete Counting Cocktail 3a70B (Research Products International Corp.) and analyzed by liquid scintillation. To normalize binding between samples, the total volume of 5′-^{32}P-end-labeled RNA used in individual reactions was spotted onto a dry filter membrane, quantified for every titration series, and assigned a value of 100% bound. All binding reactions were carried out in triplicate.

Quantitative Ni-NTA Agarose Bead Binding Reactions. One hundred microliter binding reactions were prepared as detailed above. Following 15 min of incubation at 65 °C, 20 μL of a 50% slurry of Ni-NTA agarose beads (Qiagen), which had been preequilibrated in binding buffer (20 mM K-Hepes pH 7.5, 100 mM KCl, 5 mM $MgCl_2$, 1 mM DTT, 0.1 mM EDTA and 10% glycerol) was added. The binding capacity of 10 μL of Ni-NTA beads is ~3−5 nmol, thus the Ni-NTA binding sites were in ~30−50-fold molar excess over SRP54 or SRP54M at the highest concentrations used. Reactions were incubated with beads on ice for 30 min. followed by spin filtering with Spin-X 0.2 μm micro filters (Costar) and washing with 200 μL (20 vol) of the binding buffer described above. The relative amount of free and bound RNA was measured by counting the Cerenkov radiation on the beads and in the washes.

Chemical Modification. Binding reactions for both diethylpyrocarbonate (DEPC) modification and hydroxyl radical cleavage experiments were carried out in 20 mM K-Hepes (pH 7.5), 100 mM KCl, 5 mM $MgCl_2$, 1 mM DTT, 0.1 mM EDTA and 2 mg/mL tRNA with 5′-32P-end-labeled-7S RNA (<15 nM) and either ~100 nM SRP19 and/or SRP54 or ~1 μM SRP54M (for M-domain alone reactions) or ~500 nM SRP54M (for SRP19 + SRP54M reactions) in a final volume of 20 μL. Protein samples were spin-dialyzed in Centricons with a 3000 molecular weight cut off (Amicon) against binding buffer to remove glycerol, which can quench hydroxyl radicals. All initial binding reactions were equili-

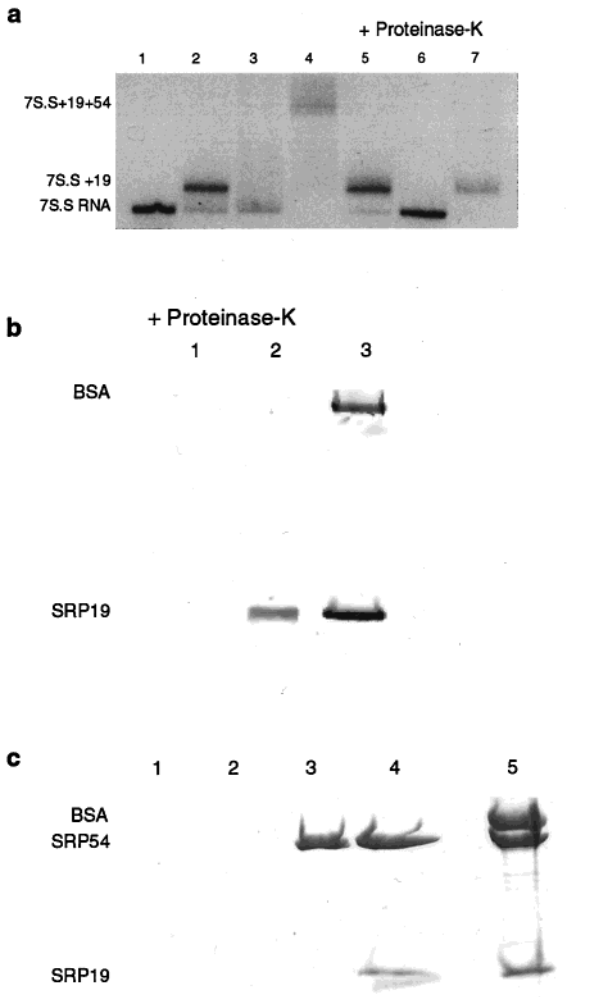

FIGURE 2: (a) Susceptibility of *A. fulgidus* SRP complexes to treatment with proteinase-K. Lanes 1−4 are native gel mobility shift experiments (Materials and Methods) with a second incubation for 15 min at 37 °C with 1 μL of 20 mM $CaCl_2$. Lanes 5−7 are identical to lanes 2−4 except that they include 1 μL of 20 mg/mL proteinase-K in 20 mM $CaCl_2$, which is required for optimal proteinase-K activity. Lane 1, trace 5′-^{32}P-end-labeled 7S.S RNA only; lanes 2 and 5, trace 5′-^{32}P-end-labeled 7S.S RNA + 50 nM SRP19; lanes 3 and 6, trace 5′-^{32}P-end-labeled 7S.S RNA + 1 μM SRP54; lanes 4 and 7, trace 5′-^{32}P-labeled 7S.S RNA + 50 nM SRP19 + 50 nM SRP54. (b) Reactions of SRP19 and BSA with proteinase-K in the absence (lane 1) and presence (lane 2) of 7S.S RNA. Both reactions also contained 1 mg/mL tRNA as a competitor. Lane 3 is a control with total untreated protein used in protease reactions. Reactions were fractionated via 15% SDS−PAGE and stained with Coomassie. (c) 7S.S RNA dependent formation of archaeal SRP complexes as shown by the ability of SRP19 to associate with Ni-NTA agarose beads only in the presence of both his-6-tagged-SRP54 and 7S.S RNA. Binding reactions in lanes 1−4 all contain 1 mg/mL tRNA and 1 μM BSA. Lane 1, SRP19; lane 2, SRP19 + 7S.S RNA; lane 3, SRP19 + SRP54; lane 4, SRP19 + 7S.S RNA + SRP54. Lane 5 is a control lane with total untreated protein used in binding reactions. Reactions were fractionated via 15% SDS−PAGE and stained with Coomassie.

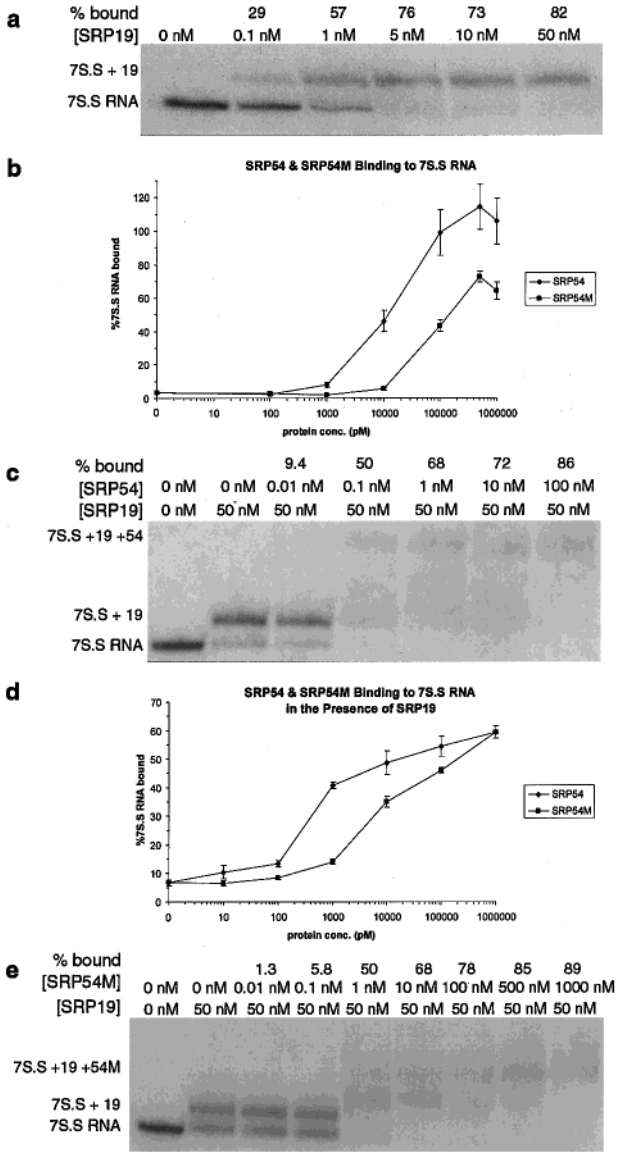

FIGURE 3: Quantification of *A. fulgidus* SRP protein/RNA complex formation. All reactions were preequilibrated at 65 °C for 15 min prior to loading on gels and contained 1 mg/mL tRNA and 1 mg/mL BSA as competitors (see Materials and Methods). (a) Native gel mobility shift assays of SRP19/7S.S RNA complexes. Apparent K_Ds for all mobility shift experiments are estimated as the protein concentration where 50% of the RNA is shifted into the lower mobility band as measured by phosphorimager. A titration of trace 5′-32P-end-labeled-7S.S RNA with SRP19 is shown. (b) Nitrocellulose filter binding experiments for complexes of SRP54 and SRP54M with trace 5′-32P-end-labeled-7S.S RNA. All filter binding reactions were washed with 250 reaction volumes of binding buffer to increase specificity and reduce background. All binding curves were done in triplicate and plotted on a semilogarithmic scale with apparent K_Ds estimated as the protein concentration at which half-maximal binding is observed. (c) Native gel titration of SRP54 against trace 5′-32P-end-labeled-7S.S RNA at constant SRP19 concentration (50 nM). (d) Ni-NTA agarose bead binding experiments for complexes of SRP54 and SRP54M binding to complexes of SRP19 and trace 5′-32P-end-labeled-7S.S RNA. Since SRP54 and SRP54M but not SRP19 possess a 6-histidine tag, complexes of SRP54{SRP19/7S.S RNA} and SRP54M{SRP19/7S.S RNA} may be separated from free SRP19/7S.S RNA complexes via binding to Ni-NTA agarose beads. Titrations of SRP54 and SRP54M against trace 5′-32P-end-labeled-7S.S RNA at constant SRP19 concentration (50 nM) are shown. Apparent K_Ds were estimated as described above for filter binding experiments. (e) Native gel titration of SRP54M against trace 5′-32P-end-labeled-7S.S RNA at constant SRP19 concentration (50 nM).

brated at 65 °C for 15 min followed by modification reactions. Modifications were done as previously described (*41*−*43*). Hydroxyl radicals were generated with freshly prepared 1 mM iron II ammonium sulfate, 2 mM EDTA, 10 mM ascorbate, and 0.025% H_2O_2. Reactions were incubated on ice for 10 min then quenched with an equal volume of 100 mM thiourea, 0.6 mg/mL glycogen, 50 mM EDTA, and 1% SDS followed by extraction with phenol, chloroform, and ethanol precipitation.

One microliters of neat DEPC was added to binding reactions and incubated at room temperature for 10 min. Reactions were quenched with 1 μL of 10 mg/mL tRNA and 6 μL of 5 M NaCl followed by ethanol precipitation. Modified RNA pellets were resuspended in 20 μL of 1 M aniline acetate and incubated at 55 °C in the dark for 20 min followed by ethanol precipitation. Bands were assigned based on mobility relative to bands in alkaline hydrolysis and RNAse T1 (G) ladders (*41*). All reactions were resuspended in 5 μL of deionized water and either 50% deionized formamide or 10 M urea, 2 μL of which was then fractionated on an 8% denaturing polyacrylamide gel and visualized by autoradiography.

Model Building and Molecular Graphics. The model for helix 6 of 7S RNA was built from three separate fragments. The first, comprising residues G138-C146 and G170-A175, was generated using a torsion angle molecular dynamics protocol to prepare a standard A-form RNA helix (*44*). The conformation of the bulged C at position 150 was extracted from the crystal structure of the MS2 viral capsid bound to an RNA operator (PDB identifier 1AQ3) (*45*). Finally, residues G151−C172 of helix 6 were obtained from a similarly structured region of the P4−P6 domain of the group I intron (PDB identifier 1GID) (*46*). UCSF Midas was used to manually dock the fragments together and to modify the bases to fit the SRP RNA sequence (*47*, *48*). RNA backbone geometry was regularized using the Crystallography and NMR System (CNS) (*49*). Molecular images were rendered using the program Ribbons 3.0 from the Center for Macromolecular Crystallography at the University of Alabama, Birmingham.

RESULTS

RNA Binding Assays. We have used native gel mobility shift, filter binding, and Ni-NTA agarose bead binding assays to estimate the affinities of archaeal SRP19 and SRP54 proteins for *A. fulgidus* SRP RNA and the role of SRP19 in the formation of SRP54−SRP RNA complexes. In all of the experiments presented here we have used a truncated version of the *A. fulgidus* 7S RNA corresponding to the signal-binding domain, that we refer to as 7S.S RNA (Figure 1). All binding experiments contained 1 mg/mL tRNA and 1 mg/mL bovine serum albumin (BSA) to ensure that observed binding was highly specific (see Materials and Methods). As shown in Figure 2a lanes 1, 2, and 4, 7S.S RNA, 7S.S RNA /SRP19, and 7S.S RNA/SRP19/SRP54 complexes are readily resolved using native polyacrylamide gel electrophoresis. As shown in Figure 2a, lane 2, and previously (*16*), SRP19 alone is competent to bind to 7S.S RNA. Furthermore SRP54 has been shown (*16*) and can be seen to bind to 7S.S RNA in Figure 2a, lane 3, despite the lack of a single shifted band, by the shifting of radioactivity to lower mobility species and the reduction of the observable amount of free 7S.S RNA.

It has been previously reported that human SRP RNA exists in two stable conformations as resolved by native gel electrophoresis, one of which has a ~3.5-fold higher affinity for SRP19 over the other (*50*). It is worth noting that under our native gel conditions, we only observe a single band for 7S.S RNA alone (Figure 2a, lane 1) and for full length 7S RNA (data not shown). However, it remained a formal possibility that the lower mobility bands observed in our gel assays were not protein−RNA complexes but rather stable alternative RNA conformers induced by transient interactions with proteins. To directly test this hypothesis, we used proteinase-K, a sequence non-specific protease (*51*), to remove proteins from the proposed SRP complexes prior to analysis by native gel electrophoresis. Figure 2a, lanes 6 and 7, show that, as expected, treatment with proteinase-K eliminates any mobility shifts attributed to the presence of SRP54. Surprisingly, shifted RNA bands attributed to the presence of SRP19 appear to be unaffected by the presence of proteinase-K (compare lanes 2 and 4 with lanes 5 and 7 in Figure 2a). Furthermore, treatment of the ternary complex of SRP54/SRP19/7S.S RNA with proteinase-K yields a complex with a mobility matching that of the apparent SRP19/7S.S RNA complex (Figure 2a, lane 4 vs lane 7). To better understand the unexpected proteinase-K resistance of the proposed SRP19/7S.S complexes, we analyzed the effect of proteinase-K on SRP19 in the absence and presence of 7S.S RNA by SDS−PAGE. Both SRP19 and BSA are degraded by proteinase-K when mixed together with 1 mg/mL tRNA (Figure 2b, lane 1). However, as shown in Figure 2b, lane 2, addition of equimolar concentrations of 7S.S RNA (relative to SRP19) significantly protects SRP19 from proteinase-K while not effecting BSA degradation. The reduced susceptibility to proteolysis upon association with the RNA could result from either SRP19-folding into a more stable, compact structure or from its burial within the RNA complex. Finally, as shown in Figure 2c, association of SRP19 with SRP54 is both highly specific and 7S.S RNA dependent, since nonspecific components such as BSA and tRNA do not associate with SRP54 or promote association of SRP19 with SRP54 respectively (Figure 2c, lane 3). Only addition of 7S.S RNA (Figure 2c, lane 4) promotes nearly quantitative association of SRP19 with SRP54. Upon the basis of these results, we conclude that the observed mobility shifts are in fact bona fide protein−RNA complexes.

As shown in Figure 3a, SRP19 binds to 7S.S RNA with high affinity and specificity. Apparent protein−RNA equilibrium dissociation constants (K_Ds) can be estimated from the protein concentration at which ~50% of the trace labeled RNA ([RNA] < 0.1[protein]) is shifted into the lower mobility form (*52*). SRP19 tightly binds 7S.S RNA with an apparent K_D of ~1 nM.

To quantitatively assess the role of SRP19 in archaeal SRP assembly, it was important to first measure the affinity of SRP54 for 7S.S RNA in its absence. In contrast to the discrete low mobility complex observed for SRP19/7S.S RNA, SRP54 produced a continuous smear of lower mobility species as shown in Figure 2a, lane 3, and as seen previously (*16*). Formation of the shifted 7S.S/SRP54 complexes was dependent on the cross-linker concentration in the native gels. Since the mobility shift assay is a nonequilibrium technique, influenced by the degree of macromolecular "caging" within the native gel matrix, complexes with rapid association/dissociation kinetics often cannot be experimentally detected by traditional native gel mobility shift methods [e.g., λ repressor−operator DNA (*53*)]. As an alternative independent measure, we used nitrocellulose filter binding in an effort to determine the same parameter. As measured by this technique, the apparent K_D of SRP54 for 7S.S RNA is estimated as the point of half-maximal binding and is ~15 nM (Figure 3b). SRP54 alone clearly has significant affinity for 7S.S RNA, quite unlike its eukaryotic homologues (*15*, *54*). The apparent K_D for formation of the SRP19/7S.S RNA complex as determined by filter binding is ~1 nM (not shown), identical to that obtained using the gel mobility shift assay, lending further support to the validity of both methods. Both filter binding and mobility shift assays were also carried out using 7S RNA. Measured binding constants for the full length RNA were indistinguishable from those obtained for the S-domain RNA fragment (data not shown).

Table 1: Summary of *A. fulgidus* SRP Protein/RNA Binding Data

complex	technique	apparent K_D (nM)
SRP19/7S.S RNA	native gel	1
SRP54/7S.S RNA	filter binding	15
SRP54/{SRP19/7S.S RNA}	native gel	0.1
SRP54/{SRP19/7S.S RNA}	Ni−NTA bead binding	0.5
SRP54M/7S.S RNA	filter binding	60
SRP54M/{SRP19/7S.S RNA}	native gel	1
SRP54M/{SRP19/7S.S RNA}	Ni−NTA bead binding	8

The apparent K_D of SRP54 for a complex of SRP19 and 7S.S RNA as determined by native gel mobility shift is ~0.1 nM (Figure 3c). Since SRP54, but not SRP19, has a hexahistidine tag, we were able to separate free 7S.S/19 complexes from 7S.S/19/54 complexes using Ni-NTA agarose beads (see Materials and Methods). As shown in Figure 3d, the apparent K_D of SRP54 for the complex of SRP19 and 7S.S RNA as determined by the Ni-NTA bead binding assay is ~0.5 nM, in good agreement with the mobility shift data. As a final control, we repeated the SRP54/7S.S RNA binding assay with Ni-NTA beads but without SRP19 and estimated an apparent K_D of ~20 nM in close agreement with the filter binding data (not shown). On the basis of the binding data shown in Figure 3 and summarized in Table 1, *A. fulgidus* SRP19 induces an ~30−150-fold increase in the affinity of SRP54 for 7S.S RNA.

SRP54 has a universally conserved domain structure that includes an amino terminal domain with GTPase activity (NG-domain) and a carboxy-terminal methionine-rich domain responsible for signal peptide binding (M-domain). While the M-domain appears to be the primary determinant for SRP−RNA binding (*25*, *26*, *36*), removal of the NG-domain from the *M. mycoides* SRP54 homologue causes a 5-fold decrease in affinity for SRP RNA, suggesting that the NG-domain provides additional RNA binding determinants (*33*). To determine the role, if any, of the NG-domain of SRP54 in the assembly of SRP54/SRP RNA complexes, we measured assembly of SRP complexes using a truncated version of SRP54 containing only the M-domain (SRP54M). A comparison of filter binding data for the full-length *A. fulgidus* and M-domain proteins is shown in Figure 3b. The apparent K_D for the SRP54M/7S.S RNA complex is ~60 nM, corresponding to an ~4-fold decrease in RNA affinity upon removal of the NG-domain of SRP54. Apparent K_Ds

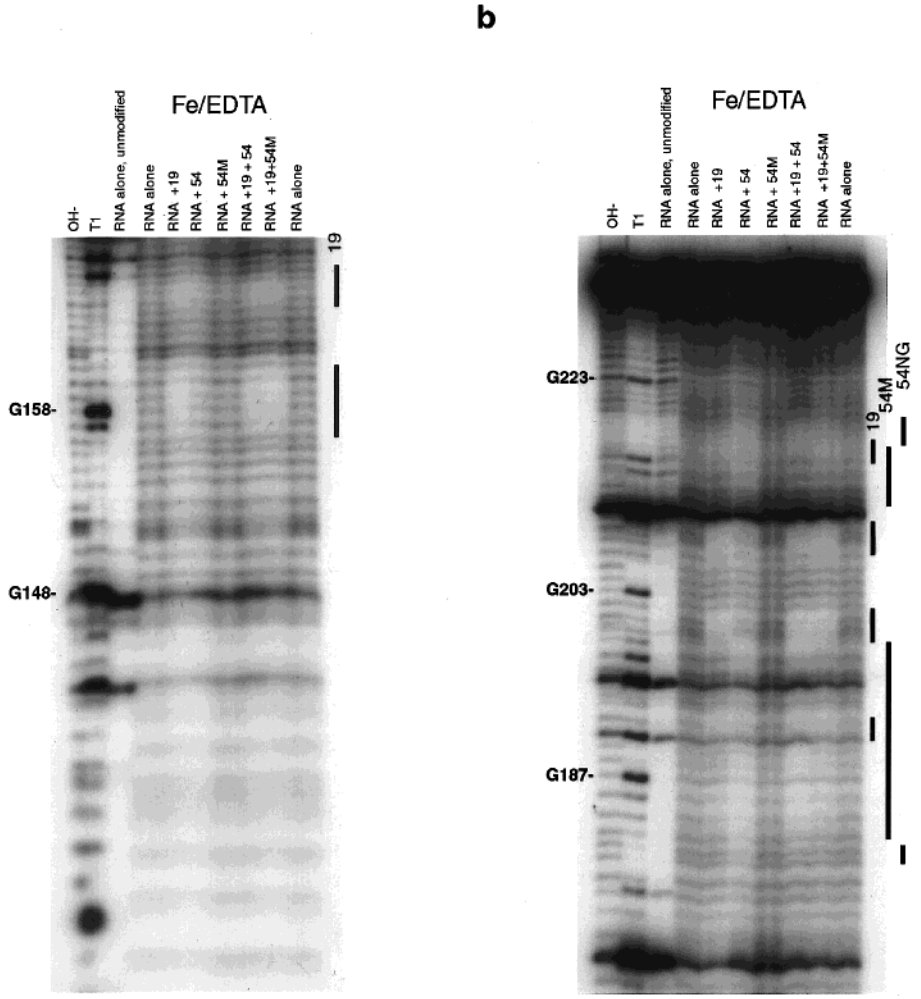

FIGURE 4: Hydroxyl radical (Fe/EDTA) modification reactions of complexes with 7S.S RNA. Reactions of 7S.S RNA alone and in complex with SRP19, SRP54, SRP54M, SRP19 & SRP54, and SRP19 and SRP54M, along with sequencing lanes (OH-, cuts every base and RNase T1, cuts at G). Positions of differential modification are indicated with solid bars. (a) Short run (50 min at 75 W). (b) Long Run (2 h at 75 W). (see Materials and Methods for further experimental details)

of 1 nM and 8 nM were measured for SRP54M binding to complexes of SRP19/7S.S RNA and 7S.S RNA, respectively. Thus, there is an SRP19-dependent increase in SRP54M/7S.S RNA affinity of ~8−60-fold. Furthermore, there is an NG-domain-dependent decrease in affinity of ~10−16-fold for SRP19/SRP54M/7S.S RNA (Figure 3, panels d and e, and Table 1). Thus while the M-domain of *A. fulgidus* SRP54 binds with high specificity and relatively high affinity to SRP RNA, the NG-domain also contributes to RNA binding, consistent with previously published results for a bacterial SRP (*33*). Furthermore, the relative enhancement of SRP54 binding to RNA induced by SRP19 is slightly increased relative to that measured for the M-domain construct.

Chemical Modification. Having shown that the archaeal SRP components assemble to form a stable complex analogous to that of their eukaryotic homologues, chemical probing experiments were undertaken to map the binding sites of SRP19, SRP54, and SRP54 M-domain on 7S.S RNA. As seen in Figure 4, all experiments containing protein with the exception of those containing SRP54M alone give clear and distinct protections of 7S.S RNA from hydroxyl radicals. As shown in Figure 5, the *A. fulgidus* 7S.S construct is not highly susceptible to modification by diethylpyrocarbonate (DEPC), as previously observed for 4.5S RNA (*55*). Since DEPC most strongly modifies the N7 position of adenine (*41*, *43*), we cannot make conclusions about base pairing, but can infer that the majority the adenosine bases in 7S.S RNA are stacked. Finally, the modification pattern of 7S.S RNA in the absence of magnesium was essentially identical to that of the RNA in its presence, suggesting that divalent cations alone do not induce large scale tertiary folding of the RNA (data not shown).

A summary of all protections and modifications that we observe is shown in Figure 6. SRP19 effects can be considered in two classes. The first class is defined by strong protections from hydroxyl radicals, which represent a primary binding site for the protein. The second class is defined by somewhat weaker protections from hydroxyl radicals and exposures to DEPC, which we interpret as indirect effects of SRP19 binding to 7S.S RNA, reflecting RNA−RNA interactions and conformational changes distant from the SRP19 primary binding site.

SRP19 strongly protects regions at the distal ends of both helix 6 and helix 8, in good agreement with predictions for the binding site for human SRP19 on human 7S RNA based on mutagenesis of the RNA (*27*, *28*, *36*) and previously reported protection studies (*15*). There is a weak DEPC modification observed at position A205, which is protected

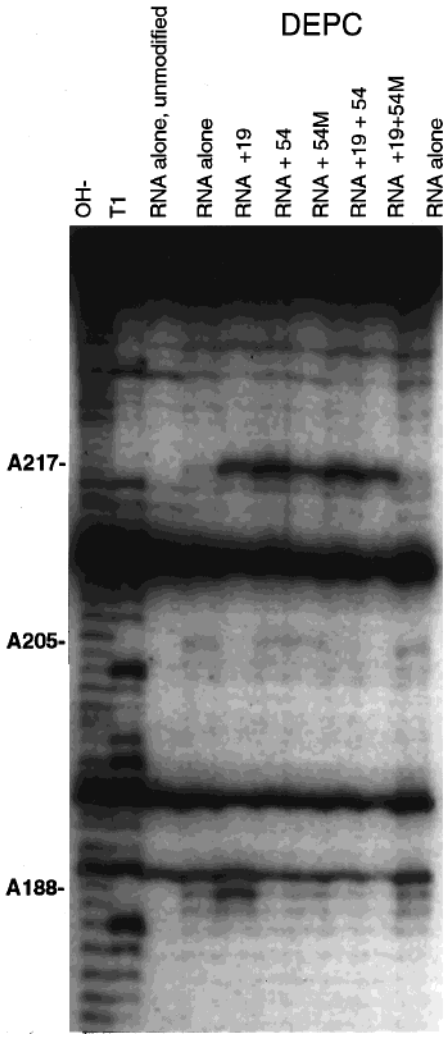

FIGURE 5: DEPC modification reactions of complexes with 7S.S RNA. Reactions of 7S.S RNA alone and in complex with SRP19, SRP54, SRP54M, SRP19 and SRP54, and SRP19 and SRP54M, along with sequencing lanes (OH-, cuts every base and RNase T1, cuts at G). Run 2 h at 75 W (see Materials and Methods for further experimental details).

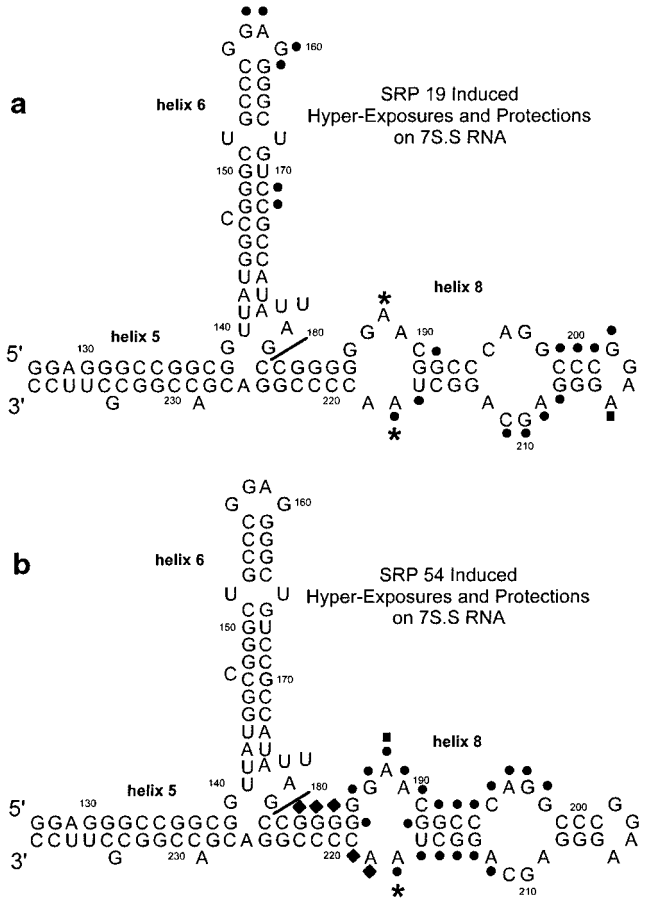

FIGURE 6: Summary of protections from and exposures to modification reagents on 7S.S RNA. (a) Protections and exposures to modification reagents attributed to SRP19. Black circles indicate protection from hydroxyl radicals while filled squares and stars indicate protection from and exposure to DEPC, respectively. (b) Protections and exposures to modification reagents attributed to SRP54. Black circles indicate protection from hydroxyl radicals attributed to SRP54M while black diamonds indicate protection from hydroxyl radicals attributed to SRP54-NG. Filled squares and stars indicate protection from and exposure to DEPC, respectively.

by SRP19 yet appears to lie outside the binding site based on the hydroxyl radical footprint in that region (Figures 5 and 6a). This weak modification/protection is probably the result of SRP19 stabilizing the G·A base pairing (which includes a G amino-A N7 hydrogen bond observed in GNRA tetra-loops generally (*56*) and in this tetra-loop specifically (*19*)) via interaction at position G202. Thus we identify positions G158-G161 on helix 6 and C199-G202 and G208-C211 on helix 8 as the primary binding sites for SRP19.

SRP19 appears to influence the structure of 7S.S RNA in regions distinct from its proposed primary site of interaction. The most striking of these effects are dramatic increases in DEPC modification and protections from hydroxyl radicals in the asymmetric bulge of helix 8 (shown in Figures 4b and 5 and summarized in Figure 6a). From the DEPC exposures at positions A188 and A217 we infer that the structure of the asymmetric bulge of helix 8 is changed upon binding of SRP19. Additional protections from hydroxyl radicals on helix 6 in the region of C168 and C169 could be the result of SRP19 induced RNA/RNA interactions between helix 6 and helix 8 (Figures 4a and 6a). Finally, there are protections from hydroxyl radicals in regions surrounding G191 and U216-A217 (Figures 4b and 6a). Since these positions are within and directly adjacent to the asymmetric bulge, and are also protected by SRP54 alone (see below), it is likely that they are induced by the same conformational change that causes the DEPC exposures at positions A188 and A217.

Figure 6b summarizes the hydroxyl radical and DEPC modifications observed upon binding of SRP54 to 7S.S RNA with or without SRP19. SRP54 has its own uniquely defined binding site on 7S.S RNA, which does not overlap with the proposed primary binding sites of SRP19. Hydroxyl radical protections and DEPC protections/exposures for SRP54 on 7S.S RNA are shown in Figures 4 and 5, respectively, and summarized in Figure 6b. Position A188 is protected by SRP54 from DEPC even in the presence of SRP19 (Figures 5 and 6). Interestingly, SRP54 alone induces exposure to DEPC at position A217, suggesting that it is able to affect aspects of the conformational change in this region induced by SRP19 and possibly explaining the ability of SRP54 to bind to the SRP RNA in the absence of SRP19.

SRP54M alone does not appear to strongly protect any positions from hydroxyl radicals, which might be attributed its reduced affinity for SRP RNA (Figure 3b). It does,

however, expose position A217 to DEPC (Figures 5 and 6b), although somewhat more weakly than full length SRP54, suggesting that it is in fact binding the RNA in a mode similar to the full length protein. A comparison of the hydroxyl radical protections induced by SRP54 (alone or with SRP19) and those induced by SRP54M (with SRP19) reveals very nearly identical footprints as shown in Figure 4b. Addition of the NG-domain of SRP54 appears to extend the M-domain footprint further down helix 8, with an increase in protection in the regions of G182−G184 and A218−C219 (Figures 4b and 6b). While the increase in RNA binding affinity conferred by the NG-domain may be a result of NG-domain-dependent stabilization of the M-domain, the additional hydroxyl radical protections argue for some degree of direct NG-domain−RNA interaction. Furthermore, the extension of the protections toward A218−C219, which are within the asymmetric bulge reorganized by SRP19, might explain the difference in NG-domain RNA binding dependence in the presence or absence of SRP19, 10−16 vs 4-fold, respectively (Table 1).

Finally, there is overall good agreement between the hydroxyl radical protections observed for the *A. fulgidus* SRP54/7S.S RNA complex presented here and the *ffh*/4.5S RNA complex from *E. coli* (*55*). On the 5′-strand of helix 8 of 4.5S RNA continuous protection from hydroxyl radicals by *ffh* is observed across positions 180−199 (*A. fulgidus* numbering) with the exception of positions 189 and 190 where there were pauses in reverse transcriptase. Similarly, we observe protection from hydroxyl radicals by SRP54 across positions 182−198 (Figures 4b and 6b). On the 3′-strand of helix 8 of 4.5S RNA there are protections from hydroxyl radicals at positions analogous to 212−213, 219, and 221−222 with reverse transcriptase pauses at positions 214−217 (*55*). Again, this is quite similar to the data presented here for the *A. fulgidus* system with two exceptions. First, *ffh* has a larger hydroxyl radical footprint, extending well into the region of 4.5S RNA that is structurally analogous to helix 5 of 7S RNA. Since 4.5S RNA lacks helix 6, it is difficult to interpret the significance, if any, of this difference in protection. Second, positions in 4.5S RNA analogous to nucleotides 217 and 218 of 7S RNA are not protected by *ffh* but they are protected by SRP54 in 7S RNA (*55*) (Figures 4b and 6b). This second difference suggests that some structural differences may exist between the asymmetric bulges of *E. coli* and *A. fulgidus* helix 8.

DISCUSSION

Protections in Three Dimensions. The NMR structures of both the distal loop alone (*19*) and the asymmetric bulge and distal loops together of helix 8 from *E. coli* 4.5S RNA have been solved recently (*20*). Crystal structures of helix 8 from *E. coli* 4.5S RNA (although in a dimeric form with significant crystal contacts in the region of the asymmetric bulge) (*21*) and a helix 8 fragment bound to the M-domain of *E. coli ffh* (*24*) have also been determined recently. Comparison of RNA sequences from *E. coli* and *A. fulgidus* in the region of the distal loop of helix 8, residues G193−C214 (*A. fulgidus* numbering), reveals absolute conservation of secondary structure and nearly absolute conservation of sequence. The only differences in sequence are conservative changes in paired regions (i.e., C:G to U:A). In the region of the helix 8 asymmetric bulge, however, residues G184-G192, and C215−C220 (*A. fulgidus* numbering) the sequence identity is not as well conserved.

The chemical modification results highlight the asymmetric bulge of helix 8 as a critical region for both SRP19 induced conformational changes and SRP54 binding. This same region of 4.5S RNA has been shown to undergo radical reorganization upon binding of the M-domain of ffh as shown by comparison of structures of the free RNA and the protein/RNA complex (Figure 7, panels a and b) (*20*, *24*). As shown in Figure 7, panels a−c, the 3′-staggered hydroxyl radical protections made by SRP19 on the distal loop of helix 8 define a minor-groove face for protein binding. The noncanonical pairings in the highly conserved distal loop provide a shallow surface with a number of hydrogen bond donors and acceptors that might not be available for contact in regular A-form RNA. Figure 7b shows that the SRP19 hydroxyl radical protections on helix 8 do not significantly overlap with the M-domain binding site observed in the crystal structure (*24*). This is also consistent with the nonoverlapping protections for SRP19 and SRP54 in the same region of the archaeal RNA (Figures 4b and 6).

Analysis of the crystal structure of the core of the *E. coli* SRP led to the suggestion that signal peptide binding might depend in part upon direct interactions between the signal peptide and the RNA (*24*). In particular, basic residues at the amino terminus of the peptide were proposed to make direct contacts with the RNA phosphate backbone in the distal bulge of helix 8. It is interesting to note that the SRP19 protections at positions 199−201 overlap with this putative contact site. Higher resolution structural data is required to determine whether SRP19 binding actually prevents direct contacts between the signal peptide and the RNA in the archaeal particle. Interestingly, integral membrane protein signal peptides from *Archaeal* bacteriorhodopsin homologues generally lack the N-terminal positively charged amino acids common in *Bacteria* (*11*). Furthermore, analysis of signal sequences from *Eukarya*, which like *Archaea* also possess SRP19, shows a greatly reduced frequency for positively charged amino acids at the N-terminus of signal sequences relative to those in *Bacteria* (*57*). Since the *E. coli* system lacks SRP19 altogether, it is possible that the modes of signal peptide recognition are subtly different across domains, despite the very high degree of sequence and secondary structure conservation in that region of SRP RNA.

SRP19-induced conformational changes in the asymmetric bulge of helix 8 likely reorganize at least part of that bulge in a manner that eukaryotic and archaeal SRP54 alone cannot. Residue A188, a phylogenetically conserved adenosine (*9*, *20*, *24*) is hyperexposed to DEPC upon SRP19 binding, but protected in the presence of SRP54. This adenosine is shown to make direct contacts with both protein and RNA in the *E. coli* crystal structure (*24*) and is in a very different conformation relative to the free RNA (*20*) (Figure 7, panels a and b). As seen in Figure 7b, in the crystal structure, A188 (A39 in the *E. coli* numbering) is protected from solvent by interactions with protein, but in a "protein-bound RNA structure" shown in the absence of protein (Figure 7c), A188 would be highly accessible to attack by DEPC. This suggests that the "SRP19 bound" state of the *A. fulgidus* 7S RNA proximal to residue A188 might be analogous in three-dimensional structure to the "M-domain bound" state observed in the crystal structure (*24*). This type of preorgani-

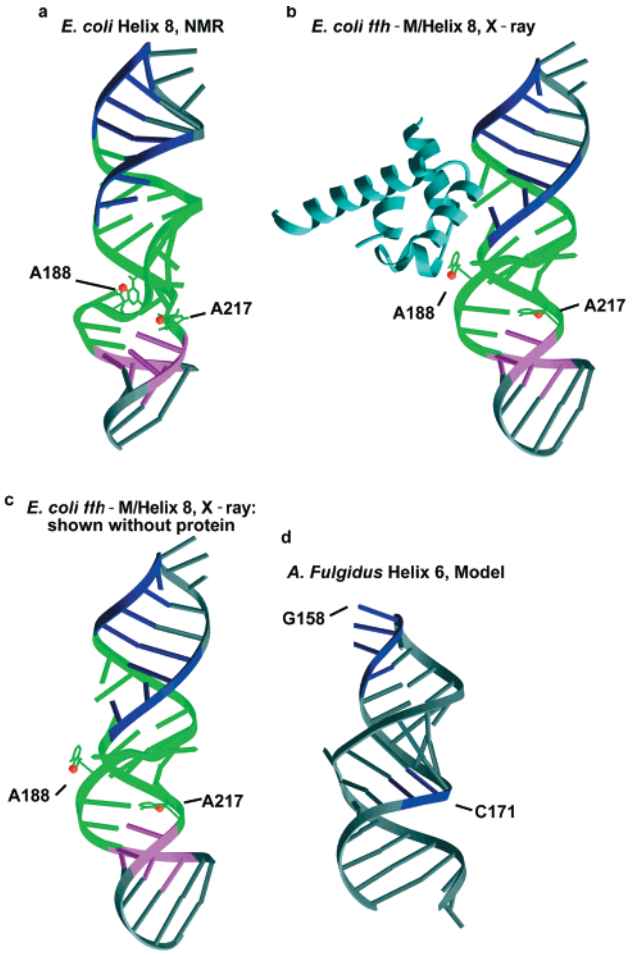

FIGURE 7: Chemical probing data visualized in three dimensions. Protections from hydroxyl radicals are indicated by coloration for each protected residue. SRP19 induced hydroxyl radical protections are shown in blue. SRP54 M-domain hydroxyl radical protections are shown in green. SRP54 NG-domain protections are shown in magenta. Positions of DEPC exposure (A188 N7 and A217 N7, *A. fulgidus* numbering) are shown in red. The M-domain protein structure is shown in cyan. (a) Ribbon representation of the *E. coli* helix 8 RNA in solution by NMR (*20*). (b) Ribbon representation of the *E. coli* SRP protein RNA complex crystal structure shown in the same orientation as the helix 8 NMR structure shown in panel a (*24*). SRP19 and SRP54M binding sites are proximal but nonoverlapping in good agreement with protection data. (c) Ribbon representation of the RNA alone from the protein/RNA complex oriented as shown in panel b. A188 N7 is clearly exposed for DEPC modification, while A217 N7 appears protected within the RNA helix. (d) Ribbon representation of a model of *A. fulgidus* helix 6 RNA.

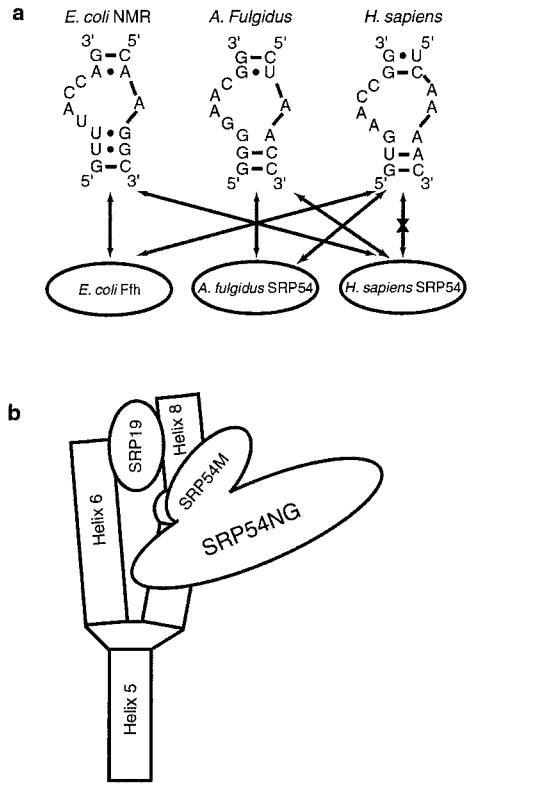

FIGURE 8: (a) Schematic representation of the secondary structures of the asymmetric bulge of helix 8 of SRP RNA across the three domains of life. The *E. coli* secondary structure is based on the NMR structure and represents the free-RNA form (*20*). The ability of SRP54 homologues to bind to various SRP RNAs is indicated with arrows. (b) Schematic model of the signal binding domain of *A. fulgidus* SRP.

zation of a binding site would certainly contribute to the SRP19 induced high affinity binding of 7S RNA by SRP54.

Interestingly, *A. fulgidus* 7S RNA residue A217, is exposed to DEPC in all protein bound states (Figures 5 and 6). However, the N7 of the equivalent residue in the crystal structure, A68 (*24*), does not appear accessible to DEPC attack (Figure 7, panels b and c). In previous chemical probing experiments in the *E. coli* system, the Watson−Crick face of A68 is highly reactive to dimethyl sulfate (DMS) in the free-RNA state and strongly protected in the protein-bound state (*55*). These results are consistent with both the free RNA NMR structure (*20*) and the protein bound crystal structure (Figure 7, panels a and b) (*24*). DMS probing of adenine N1 (*55*) and DEPC probing of adenine N7 cannot be directly compared. However, the differences in chemical reactivity of these nucleotides to both base specific probes and hydroxyl radicals (see Results), as well as differences in primary sequence (Figure 8a) suggests that while some aspects of asymmetric bulge structure are conserved across domains, others that may play a critical role in archaeal SRP54 binding may not be.

The hydroxyl radical protections observed for both the *E. coli* SRP RNA (*55*) and for the *A fulgidus* SRP RNA upon addition of SRP54M extend well beyond the direct contact site defined by the *E. coli* crystal structure (*24*) (Figure 7b). The crystallographically observed reorganization of the asymmetric bulge that is induced by SRP54M (Figure 7, panels a and b) likely explains the protections of nucleotides 189−195. As two RNA strands of the asymmetric bulge are brought into close proximity, several bases are flipped out and the corresponding ribose phosphate backbone is turned inward. RNA-RNA contacts with helix 6 could also account for some of the additional protections observed on helix 8. The additional NG-domain specific contacts on helix 8 (Figures 4, 6b, and 7, panels b and c) appear to continue along the minor groove face of the RNA and may provide for the observed increase in RNA affinity when compared to SRP54M alone.

Figure 7c shows a three-dimensional model for helix 6 of 7S RNA, generated as described in Materials and Methods. Our model is essentially an A-form helix with G138-U140 dangling beneath, C147 bulged out, U152 and U165 paired in an unspecified form, and the G157-G160 loop in the form of a GNRA tetra-loop. While single nucleotide bulges and

non-Watson−Crick pairings can be found in many archaeal helix 6 sequences, their positions and identities are not highly conserved (*8*, *9*). As such, the recently determined structure of a dimeric form of helix 6 from human SRP RNA does not directly serve as a useful model for the *A. fulgidus* helix 6 (*58*). Since the human helix 6 RNA crystallized as a duplex, there is no information about the structure of the unusual GGAG- tetraloop, which is conserved between *A. fulgidus* and *H. sapiens*. Figure 7c shows the hydroxyl radical protections from SRP19 mapped onto the model for helix 6. The SRP19 dependent protections in the middle of the helix (C171 and C172) might also be the result of RNA/RNA interactions with helix 8 induced by simultaneous binding of both helices by SRP19.

Model for Signal Binding Domain Structure, Assembly, and Evolution. The property of the archaeal SRP54 to bind to 7S RNA independent of SRP19 has made it possible to directly compare and contrast SRP19/RNA, SRP54/RNA, and SRP19/SRP54/RNA complexes and thereby assess the role of SRP19 in SRP assembly. *A. fulgidus* SRP19 alone induces hydroxyl radical protections at or near the tips of helices 6 and 8, identifying these regions as the primary SRP19 binding sites (Figures 4, 6, and 7). At the same time, SRP19 induces exposures to DEPC in the asymmetric bulge of helix 8, arguing for an SRP19 induced conformational change in this region of the RNA.

SRP54 (alone or in complex with SRP19) protects the asymmetric bulge of helix 8, nucleotides flanking the asymmetric bulge, and nucleotides in the distal loop of helix 8. The proximity of the SRP19 and SRP54 footprints on the RNA might suggest possible protein−protein interactions. However we have been unable to detect any such interactions by a variety of methods. Ni-NTA agarose beads are unable to specifically pull down SRP19 via his-6-tagged SRP54 without 7S.S RNA, although addition of 7S.S RNA yields nearly quantitative pull down of SRP19 (Figure 2c). Furthermore, clear and reproducible glutaraldehyde cross-links between SRP19 and SRP54 either with or without RNA are not observed (data not shown). Together these results suggest that SRP19 drives conformational changes in the asymmetric bulge of helix 8 combined with movement of helix 8 relative to helix 6 which allow high affinity binding of SRP54 to the RNA.

SRP19-induced conformational changes in the helix 8 asymmetric bulge could in principle arise from direct interactions between the RNA and the protein or, alternatively, as an indirect result of a long-range conformational change. The chemical modification data do not support SRP19 directly binding to 7S RNA near the asymmetric bulge of helix 8. On the other hand, simultaneous binding of SRP19 to the ends of both helix 6 and helix 8 could force a large conformational change in the RNA that translates into a localized change in the asymmetric bulge of helix 8. Solution small-angle X-ray scattering experiments indicate a >20% increase in the radius of gyration and, thus, a significant change in the overall shape of 7S.S RNA upon addition of SRP19. This observation is consistent with the proposal that SRP19 reorganizes the relative positions of helix 6 and 8 (J.L.D., Millet, Doniach, and C.W., manuscript in preparation). The protection of SRP19 from proteinase-K digestion by 7S.S RNA further suggests that SRP19 is actually nestled between helices 6 and 8 and thus protected from exposure to the protease. Helix 8 is clearly longer than helix 6 (Figures 1 and 7) and since both helices are joined covalently at the bottom, it is likely that helix 8 bends and/or twists to some degree upon binding of SRP19. Given that the asymmetric bulge is flexible (*20*) and undergoes a conformational change upon SRP19 binding, we believe that a more rigid helix 6 may act as a brace to force the SRP19 induced change in helix 8.

Earlier models of the structure of the signal-binding domain of SRP RNA have been presented (*36*, *59*). A primary feature of these models is a tertiary interaction between residues in helix 8 and helix 5 (G202 and G203 with C235 and U236 *A. fulgidus* numbering). We see no evidence of hydroxyl radical protection which might support a helix 8−helix 5 tertiary interaction. In fact, the entire 3′-strand of helix 5 is uniformly exposed to hydroxyl radical probes as is the helix 8 tetra-loop (G202−A205), except in cases where SRP19 is bound and protects residue G202 (Figure 5b). A schematic model of the S-domain of *A. fulgidus* SRP is shown in Figure 8b. In our model, SRP19 is tucked between helices 6 and 8 to bring them into close proximity. The M-domain of SRP54 is oriented relative to SRP19 based on hydroxyl radical protections and comparison with the position of protein in the *E. coli* crystal structure (Figure 7b) (*24*). The NG-domain of SRP 54 is shown making further contacts with helix 8 based on hydroxyl radical protections (Figures 5, 6b, and 7b).

In attempting to understand the assembly of the signal-binding domain of SRP across all three domains of life, a number of observations must be considered. Both human SRP54 and *E. coli ffh* bind to the *E. coli* 4.5S RNA with K_Ds of 100 nM (*26*) and 5−50 nM (*35*), respectively. Binding of human SRP54 or its M-domain alone to 7S RNA requires SRP19 in anion exchange column binding assays (*14*, *25*, *26*, *31*, *32*, *36*). Furthermore, M-domain of human SRP54 cannot bind to mutant "4.5S-like" 7S RNAs from which helix 6 has been deleted, arguing that helix 6 does not directly inhibit human SRP54 binding to 7S RNA in the absence of SRP19 (*36*). However, the 7S RNA dependent GTPase activity of human SRP54 appears to be independent of SRP19 (*60*), suggesting that human SRP54 can associate with 7S RNA, at least at some level (possibly assisted by SRP receptor proteins?) in an SRP19 independent manner. Human SRP54M has recently been shown to bind *A. fulgidus* and *M. jannaschii* SRP RNAs and *A. fulgidus* SRP54 has been shown to bind human SRP RNA independently of human and archaeal SRP19, respectively, although with apparently reduced affinity than when appropriate SRP19 is present (*16*). Surprisingly, *ffh* appears to associate with human 7S RNA without SRP19 in *E. coli* in vivo as human 7S RNA can complement *E. coli* strains depleted of 4.5S RNA (*14*). Finally, our results with SRP components from *A. fulgidus* show that while the archaeal SRP19 functionally resembles its eukaryotic homologues in its ability to promote SRP54 binding to 7S RNA, the archaeal SRP54 has significant intrinsic affinity for 7S RNA (apparent $K_D \sim 15$ nM). The ability of various SRP54 homologues to interact with SRP RNAs in the three domains of life is summarized in Figure 8a.

A rooting of the tree of life using SRP54 and SRα sequences groups the *Archaea* more closely with the *Eukarya* than with the *Bacteria* (*61*). Yet comparison of the helix 8

asymmetric bulges (Figure 8a) shows stronger similarity at the secondary structure level between the archaeal and bacterial structures than between the archaeal and eukaryotic structures (9, *20*). In particular, an additional nucleotide inserted in the 3′-strand of higher eukaryotic structures is absent from that strand in either *E. coli* or *A. fulgidus* RNAs. Based on analysis of SRP RNA sequences and protein content, the archaeal SRP might be considered an "ur-SRP", whose RNA components were truncated in bacterial evolution (*10*), and which acquired additional proteins in eukaryotic evolution. We propose that as SRP54 proteins diverged, subtle changes might have enhanced the ability of bacterial SRP54 to induce the required conformational change in the helix 8 asymmetric bulge and thus achieve high affinity binding. Furthermore, a more highly asymmetric "archaeal-like" helix 8 asymmetric bulge together with changes in primary sequence (relative to archaeal sequences) might yield a free-RNA structure that is better able to adopt a "high affinity" conformation for protein binding. Our proposal of a better RNA binding SRP54 in *Bacteria* would explain the ability of 7S RNA to complement 4.5S RNA deletions in *E. coli* (*14*) (and presumably for *ffh* to bind to 7S RNA). The idea that bacterial SRP RNA is also more fit to bind to SRP54, would explain the ability of mammalian SRP54 to bind to 4.5S RNA (*26*), but not to its own 7S RNA, or of its M-domain to bind to helix 6 deletion mutants of 7S RNA (*36*). Meanwhile, the archaeal SRP54 can bind to its own 7S RNA but with lower affinity than when SRP19 is present, thus retaining the properties of both the bacterial and the eukaryotic domains of life. The archaeal SRP54/7S RNA interaction may have retained a greater SRP19 independent affinity relative to eukaryotic homologues in order to increase overall SRP stability in extremes of temperature, salt and pH. While we have shown that the archaeal SRP54 binds tightly to SRP RNA in vitro, there is no evidence to suggest that this affinity is sufficient to drive RNP assembly under the normal physiological conditions common to extremophiles.

It has recently been shown that SRP19 (but not SRP54) localizes in the nucleolus with 7S RNA (*62*). It is possible that as eukaryotic SRP evolved and diverged from its archaeal homologues, it gained an increasing dependence on SRP19 (through subtle changes in both 7S RNA and SRP54) in order to compartmentalize and regulate SRP assembly. It is possible, that in contrast, as *Bacteria* evolved, SRP19 was lost as more efficient SRP54/RNA complex formation and a streamlined SRP developed.

ACKNOWLEDGMENT

We would like to thank R. Batey and J. Doudna for sharing coordinates of the crystal structure of the *ffh* M-domain/4.5S RNA helix 8 complex, and U. Schmitz for sharing the manuscript and coordinates for the *E. coli* 4.5S RNA helix 8 NMR structure prior to publication. We would also like to thank members of the Noller and Scott Labs at UCSC for many helpful discussions.

REFERENCES

1. Lutcke, H. (1995) *Eur. J. Biochem. 228*, 531−550.
2. Walter, P., and Blobel, G. (1980) *Proc. Natl. Acad. Sci. U.S.A. 77*, 7112−7116.
3. Walter, P., and Blobel, G. (1982) *Nature 299*, 691−698.
4. Woese, C., Kandler, O., and Wheelis, M. (1990) *Proc. Natl. Acad. Sci. U.S.A. 87*, 4576−4579.
5. Siegel, V., and Walter, P. (1986) *Nature 320*, 81−84.
6. Siegel, V., and Walter, P. (1988) *Cell 52*, 39−49.
7. Larsen, N., and Zwieb, C. (1991) *Nucleic Acids Res. 19*, 209−215.
8. Kaine, B. (1990) *Mol. Gen. Genet. 221*, 315−321.
9. Larsen, N., Samuelsson, T., and Zwieb, C. (1998) *Nucleic Acids Res. 26*, 177−178.
10. Althoff, S., Selinger, D., and Wise, J. (1994) *Nulceic Acids Res. 22*, 1933−1947.
11. Gropp, R., Gropp, F., and Beltach, M. (1992) *Proc. Natl. Acad. Sci. U.S.A. 89*, 1204−1208.
12. Walter, P., and Blobel, G. (1983) *Cell 34*, 525−533.
13. Poritz, M., Bernstein, H., Strub, K., Zopf, D., Wilhelm, H., and Walter, P. (1990) *Science 250*, 1111−1117.
14. Ribes, V., Romisch, K., Giner, A., Dobberstein, B., and Tollervey, D. (1990) *Cell 63*, 591−600.
15. Siegel, V., and Walter, P. (1988) *Proc. Natl. Acad. Sci. U.S.A. 85*, 1801−1805.
16. Bhuiyan, S., Gowda, K., Hotokezaka, H., and Zwieb, C. (2000) *Nucleic Acids Res. 28*, 1365−1373.
17. Clemons, W. J., Gowda, K., Black, S., Zwieb, C., and Ramakrishnan, V. (1999) *J. Mol. Biol. 292*, 697−705.
18. Montoya, G., te Kaat, K., Moll, R., Schafer, G., and Sinning, I. (2000) *Structure 8*, 515−525.
19. Schmitz, U., James, T., Lukavsky, P., and Walter, P. (1999) *Nature Struct. Biol. 6*, 634−638.
20. Schmitz, U., Behrens, S., Freymann, D., Keenan, R., Lukavsaky, P., Walter, P., and James, T. (1999) *RNA 5*, 1419−1429.
21. Jovine, L., Hainz, T., Outbridge, C., Scott, W., Li, J., Sixma, T., Wonacott, A., Skarzynski, T., and Nagai, K. (2000) *Structure 8*, 527−540.
22. Freymann, D., Keenan, R., Stroud, R., and Walter, P. (1997) *Nature 385*, 361−364.
23. Keenan, R., Freymann, D., Walter, P., and Stroud, R. (1998) *Cell 94*, 181−191.
24. Batey, R., Rambo, R., Lucast, L., Rha, B., and Doudna, J. (2000) *Science 287*, 1232−1239.
25. Romisch, K., Webb, J., Lingelbach, K., Gausepohl, H., and Dobberstein, B. (1990) *J. Cell Biol. 111*, 1793−1802.
26. Zopf, D., Bernstein, H., Johnson, A., and Walter, P. (1990) *EMBO J. 9*, 4511−4517.
27. Zwieb, C. (1992) *J. Biol. Chem. 267*, 15650−15656.
28. Zwieb, C. (1994) *Eur. J. Biochem. 222*, 885−890.
29. Black, S., Gowda, K., Chittenden, K., Walker, K., and Zwieb, C. (1997) *Eur. J. Biochem. 245*, 564−572.
30. Chittenden, K., Gowda, K., Black, S., and Zwieb, C. (1997) *Plant Mol. Biol. 34*, 507−515.
31. Gowda, K., Black, S., Moeller, I., Sakakibara, Y., Liu, M., and Zwieb, C. (1998) *Gene 207*, 197−207.
32. Gowda, K., Clemons, W., Zwieb, C., and Black, S. (1999) *Protein Sci. 8*, 1144−1151.
33. Samuelsson, T., and Olsson, M. (1993) *Nucleic Acids Res. 21*, 847−853.
34. Lentzen, G., Dobberstein, B., and Wintermyer, W. (1994) *FEBS Lett 348*, 233−238.
35. Schmitz, U., Freymann, D, James, T., Keenan, R., Vinayak, R., and Walter, P. (1996) *RNA 2*, 1213−1227.
36. Gowda, K., Chittenden, K., and Zwieb, C. (1997) *Nucleic Acids Res. 25*, 388−394.
37. Hauser, S., Bacher, G., Dobberstein, B., and Lutcke, H. (1995) *EMBO J. 14*, 5485−5493.
38. Klenk, H. P., Clayton, R. A., Tomb, J. F., White, O., Nelson, K. E., Ketchum, K. A., Dodson, R. J., Gwinn, M., Hickey, E. K., Peterson, J. D., Richardson, D. L., Kerlavage, A. R., Graham, D. E., Kyrpides, N. C., Fleischmann, R. D., Quackenbush, J., Lee, N. H., Sutton, G. G., Gill, S., Kirkness, E. F., Dougherty, B. A., McKenney, K., Adams, M. D., Loftus, B., and Venter, J. C., et al. (1997) *Nature 390*, 364−70.
39. Milligan, J. F., and Uhlenbeck, O. C. (1989) *Methods Enzymol. 180*, 51−62.
40. Kohrer, C., Mayer, C., Neumair, O., Grobner, P., and Piendl, W. (1998) *Eur. J. Biochem. 256*, 97−105.

41. Kjems, J., Ejebjerg, J., and Christiansen, J. (1998) in *Laboratory techniques in biochemistry and molecular biology* (Vliet, P. v. d., Ed.) Elsevier, Utrecht.
42. Merryman, C., and Noller, H. (1998) in *RNA: Protein Interactions, A Practical Approach* (Smith, C., Ed.) pp 237−253, Oxford University Press, New York.
43. Ehresmann, C., Baudin, F., Mougel, M., Romby, P., Ebel, J., and Ehresmann, B. (1987) *Nucleic Acids Res. 15*, 9109−9128.
44. Rice, L., and Brünger, A. (1994) *Proteins 19*, 277−290.
45. van den Worm, S., Stonehouse, N., Valegard, K., Murray, J., Walton, C., Fridborg, K., Stockley, P., and Liljas, L. (1998) *Nucleic Acids Res. 26*, 1345−1351.
46. Cate, J. H., Gooding, A. R., Podell, E., Zhou, K., Golden, B. L., Kundrot, C. E., Cech, T. R., and Doudna, J. A. (1996) *Science 273*, 1678−1685.
47. Ferrin, T., Huang, C., Jarvis, L., and Langridge, R. (1988) *J. Mol. Graph. 6*, 2−12.
48. Ferrin, T., Huang, C., Jarvis, L., and Langridge, R. (1988) *J. Mol. Graph. 6*, 13−27.
49. Brünger, A. T., Adams, P. D., Clore, G. M., DeLano, W. L., Gros, P., GrosseKunstleve, R. W., Jiang, J. S., Kuszewski, J., Nilges, M., Pannu, N. S., Read, R. J., Rice, L. M., Simonson, T., and Warren, G. L. (1998) *Acta Crystallogr., Sect. D 54*, 905−921.
50. Gowda, K., and Zwieb, C. (1997) *Nucleic Acids Res. 25*, 2835−2840.
51. Ebling, W., Hennrich, N., Klockow, M., Metz, H., Orth, H. D., and Lang, H. (1974) *Eur. J. Biochem. 47*, 91−97.
52. Carey, J. (1991) in *Protein-DNA Interactions* (Sauer, R., Ed.) pp 103−117, Academic Press, San Diego, CA.
53. Lim, W., Sauer, R., and Lander, A. (1991) in *Protein-DNA Interactions* (Sauer, R., Ed.) pp 196−210, Academic Press, San Diego, CA.
54. Romisch, K., Webb, J., Herz, J., Prehn, S., Frank, R., Vingron, M., and Dobberstein, B. (1989) *Nature 340*, 478−482.
55. Lentzen, G., Moine, H., Ehresmann, C., Ehresmann, B., and Wintermeyer, W. (1996) *RNA 2*, 244−253.
56. Jucker, F., Heus, H., Yip, P., Moors, E., and Pardi, A. (1996) *J. Mol. Biol. 264*, 968−980.
57. Nielsen, H., Engelbrect, J., Brunak, S., and von Heijne, G. (1997) *Protein Eng. 10*, 1−6.
58. Wild, K., Weichenrieder, O., Leonard, G., and Cusack, S. (1999) *Structure 7*, 1345−1352.
59. Zwieb, C., Muller, F., and Larsen, N. (1996) *Folding Des. 1*, 315−324.
60. Miller, J., Wilhelm, H., Gierasch, L., Gilmore, R., and Walter, P. (1993) *Nature 366*, 351−354.
61. Gribaldo, S., and Cammarano, P. (1998) *J. Mol. Evol. 47*, 508−516.
62. Politz, J., Yarovoi, S., Kilroy, S., Gowda, K., Zwieb, C., and Pederson, T. (2000) *Proc. Natl. Acad. Sci. U.S.A. 97*, 55−60.

BI001180S